AIAA JOURNAL
Vol. 32, No. 9, September 1994

Turbulent Drag Reduction Mechanism Above a Riblet Surface

Yuji Suzuki* and Nobuhide Kasagi†
University of Tokyo, Tokyo 113, Japan

The structure of a turbulent flowfield along a riblet surface was investigated with the aid of a three-dimensional particle tracking velocimetry. The statistics of all three velocity components were measured and compared with those above a smooth wall. Under a drag-reducing condition, all of the turbulent velocity fluctuations and the Reynolds shear stress were decreased near the riblet surface, although the flow characteristics in most of the flowfield were quite similar to those above the smooth wall. It was also found that the redistribution mechanism of the turbulent kinetic energy from the streamwise component to the spanwise one was considerably suppressed in the region above the riblet valley. On the other hand, under a neutral drag condition, a cross-stream secondary flow was apparent near the ribs. This fluid motion should enhance the turbulent momentum transport and deteriorate the drag-reducing effect of the riblet.

Nomenclature

b_{ij}	= stress anisotropy tensor, $\overline{u_iu_j}/(2k) - \delta_{ij}/3$
h	= riblet height
k	= turbulent kinetic energy, $\overline{u_iu_i}/2$
L	= development length along the riblet surface
$R_{uu}(\Delta x)$, $R_{vv}(\Delta x)$, $R_{ww}(\Delta x)$	= two-point correlations in the streamwise direction
$R_{uu}(\Delta z)$, $R_{vv}(\Delta z)$, $R_{ww}(\Delta z)$	= two-point correlations in the spanwise direction
Re_m	= Reynolds number based on U_m and δ
Re_0	= Reynolds number based on U_0 and δ
s	= riblet spacing
U, V, W	= mean velocities
U_m	= bulk mean velocity
U_0	= maximum velocity
u, v, w	= velocity fluctuations
u_τ	= wall-friction velocity
x, y, z	= streamwise, wall-normal, and spanwise directions
y_p	= virtual origin
δ	= channel width at the test section
δ_0	= channel width at the developing region
ϵ	= dissipation rate of turbulent kinetic energy
ν	= kinematic viscosity
$(\ )_{\rm rms}$	= root-mean-square value
$(\ )^+$	= value nondimensionalized by u_τ and ν
$(\ )_{,i}$	= derivative with respect to x_i

I. Introduction

SINCE the 1970s, many intensive investigations have been carried out on turbulent drag reduction. Among them, the microgrooved riblet surface is believed to be one of the most promising methods for practical applications. Walsh[1] was the first to study skin-friction drag of the riblet wall systematically. He found that the triangular or scalloped riblet of which spacings are less than 25 viscous wall units can reduce the friction drag by up to 8%. Since then, many studies of the riblet surface were performed under various flow conditions, and knowledge of the drag reduction characteristics has been accumulated.[2] Hot-wire[3-5] and laser Doppler velocimetry (LDV)[6-8] measurements showed that the turbulent intensities and the Reynolds shear stress were reduced near the riblet surface. However, these techniques could not fully explore the turbulent statistics close to the riblet surface that had small spacing and height. Thus, the behavior of the statistics in the vicinity of the ribs remains unknown, and the mechanism of drag reduction is still an open question.

Recently, Choi et al.[9] carried out a direct numerical simulation (DNS) of the turbulent flow above a V-shaped riblet surface. Compared with the various DNS of channel flow by Kim et al.[10] and Kuroda et al.,[11] their calculation was performed in a rather small computational domain and on relatively coarse grids in the streamwise direction. However, they predicted the skin-friction drag in close agreement with the Walsh's data.[1] They reported that the flow characteristics depended strongly on the spacing of the ribs. Chu and Karniadakis[12] also performed a DNS of a riblet flow for $s^+ = 25.5$ by using a spectral element method. They obtained 6% drag reduction, which is somewhat larger than the experimental results.[2]

The goal of the present study is to obtain detailed turbulent statistics above a riblet surface and to deduce the drag reducing mechanism. To do this, the three-dimensional particle tracking velocimetry (3-D PTV)[13,14] was adopted, so that instantaneous spatial distributions of all three velocity components would be measured even in the near-wall region.

II. Experimental Facility and Measurement Procedures

Measurements were carried out in a turbulent water channel.[15] The channel width δ_0 and height were 80 and 800 mm, respectively. The test section was located at $65\delta_0$ downstream of the inlet, where the flow was fully developed. In the present study, one side wall of the test section was replaced with a 30-mm-thick aluminum plate on which microgrooves were machined with high accuracy. The length and span of the riblet surface were 840 and 700 mm, respectively. The surface was coated with black anodized aluminum to avoid rust and reflection on the surface. The cross section of the riblet is shown in Fig. 1. The rib spacing s and the height h were 3.5 and 2.2 mm, respectively. The bottom of the valley was aligned 0.8 mm below the upstream channel wall; thus the width δ between the riblet valley and the opposite smooth wall was 80.8 mm. The origins of the wall-normal y and the spanwise z coordinates are chosen at the bottom of the valley and the center of the peak, respectively, as shown in Fig. 1.

Received May 18, 1993; presented as Paper 93-3257 at the AIAA 3rd Shear Flow Conference, Orlando, FL, July 6-9, 1993; revision received Feb. 22, 1994; accepted for publication Feb. 22, 1994.

*Research Associate, Department of Mechanical Engineering, Hongo 7-3-1, Bunkyo-ku.

†Professor, Department of Mechanical Engineering, Hongo 7-3-1, Bunkyo-ku.

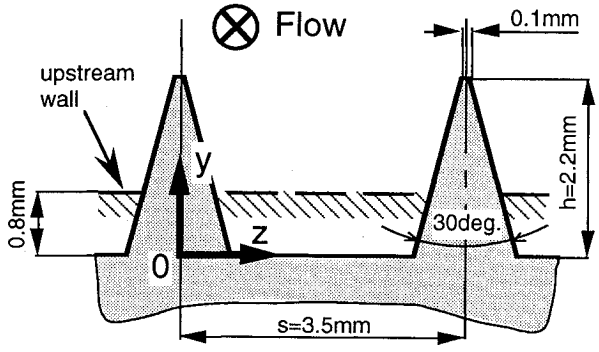

Fig. 1 Cross section of the riblet surface.

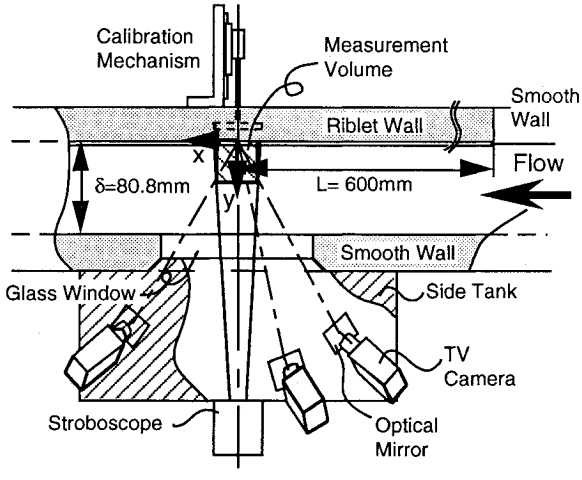

Fig. 2 Top view of the test section and camera setup.

The top view of the test section is shown schematically in Fig. 2. The measuring volume was located at 600 mm (7.5δ) downstream of the upstream end of the riblet and observed by three charge-coupled device cameras through a 20-mm-thick glass window. Zoom lenses and optical mirrors were employed to adjust the magnification of images and the viewing angles. Each lens was equipped with a waterproof cap, and the front of the cap was dipped into the side water tank to remove the effect of refraction at the window. A stroboscope synchronized with the TV signal was used for illumination. Images from each camera were recorded on a laser disk recorder. A digital image processor (NEXUS 6810, 512×480 pixels, 256 gray levels) and a workstation (Titan 3020, 64 MIPS) were used to obtain instantaneous velocity vectors from successive particle images. Details of the camera calibration procedure and the particle tracking algorithm are found in Kasagi and Nishino[13] and Sata and Kasagi,[16] respectively.

The measurements were carried out at two mean velocities; the Reynolds numbers Re_0 based on δ and the maximum velocity U_0 were about 6.05×10^3 and 1.4×10^4. This enabled us to investigate the flowfield with two different dimensionless riblet spacings as described later. Nylon 12 spherical particles, of which specific density was 1.02, were used as the flow tracers, and they were introduced into the flow at the channel inlet. The particle diameter was chosen to be 0.25 and 0.20 mm, while the time interval of image acquisition was set to be 1/30 and 1/60 s at $Re_0 = 6.05 \times 10^3$ and 1.4×10^4, respectively; they were confirmed sufficiently smaller than the Kolmogorov length and time scales. The mean flow parameters and experimental conditions are summarized in Table 1, where U_m and Re_m denote the bulk mean velocity and the Reynolds number based on δ and U_m, respectively.

The wall shear stress was not directly measured in this study, so that the wall-friction velocity estimated by the empirical correlation of Dean,[17] $u_{\tau,\mathrm{Dean}}$, is used when the viscous length scales are calculated. (The estimated values of 4.15 and 8.79 mm/s are, respectively, in reasonable agreement with those of 4.02 and 8.65 mm/s on the opposite smooth wall, which have been determined by the modified slope method.[18]) At $Re_0 = 6.05 \times 10^3$, the dimensionless spacing s^+ is about 15. Referring to Walsh,[1] the maximum drag reduction would be achieved and is estimated to be as large as 8%. On the other hand, at $Re_0 = 1.4 \times 10^4$ where s^+ is greater than 30, no drag reduction can be expected.

When $s^+ = 15$, the measurement over an about $(40\ \mathrm{mm})^3$ volume was repeated at three different wall-normal locations to obtain data over the entire channel width, while that over an about $(30\ \mathrm{mm})^3$ volume was repeated four times when $s^+ = 31$. Image acquisition was continued for 15–25 min, and about 27,000–43,000 frames were recorded at each measurement.

Uncertainty intervals associated with the instantaneous velocities measured are estimated at 95% coverage[19] as follows: For $s^+ = 15$, $u_{RSS} = 1.0$ mm/s, $v_{RSS} = 1.4$ mm/s, and $w_{RSS} = 0.83$ mm/s; for $s^+ = 31$, $u_{RSS} = 1.6$ mm/s, $v_{RSS} = 2.4$ mm/s, and $w_{RSS} = 2.4$ mm/s.

For $s^+ = 15$, an average of 270 instantaneous velocity vectors was simultaneously measured at random positions in the measuring volume, whereas 140 vectors were obtained for $s^+ = 31$. In total, 23 and 29 million instantaneous velocity vectors were obtained for $s^+ = 15$ and 31, respectively. The velocity vectors were then grouped into data cells depending on their wall-normal and spanwise positions. The wall-normal dimension of each data cell was set to be 0.25 mm. According to the spanwise periodicity, the spacing of the riblet was divided into 16 intervals (0.22 mm each). The dimensions of these cells were smaller than the Kolmogorov length scale. After this procedure, about 6000 vectors were used to obtain ensemble averages in each data cell.

Strictly speaking, the present measurement was made in the flow developing region above the riblet surface. However, the developing length L^+ is about 2500 and 5300 when $s^+ = 15$ and 31, respectively, so that the near-wall structures are believed to be sufficiently developed above the riblet surface. It is noted that the statistics separately calculated in the upstream and downstream halves of the measuring volume agree well with each other.

III. Results

A. Turbulent Statistics Above the Riblet Surface

The profiles of the streamwise mean velocity U nondimensionalized by the wall-friction velocity $u_{\tau,\mathrm{Dean}}$ are shown in Fig. 3, where $z/s = 0.0$ and 0.5 denote the spanwise locations at the peak and the center of the valley, respectively (see Fig. 1). The mean velocities above the riblet surface were plotted vs the distance from the virtual origin,[20] y_p. (The virtual origin was estimated to be 1.65 mm from a laminar flow calculation with a finite element method; the ratio of the protrusion height to the riblet spacing is about 0.157. This ratio is somewhat smaller than the value of 0.195 reported by Bechert and Bartenwerfer[20] for this configuration. This discrepancy should be due to the presence of a small plateau at the riblet peak; see Fig. 1.) With the wall-friction velocity estimated as mentioned earlier, the two velocity distributions above the smooth wall

Table 1 Mean flow parameters

	Case I	Case II
U_0, mm/s	74.8	173
U_m, mm/s	63.1	148
Re_0, $U_0\delta/\nu$	6.05×10^3	1.4×10^4
Re_m, $U_m\delta/\nu$	5.1×10^3	1.2×10^4
$u_{\tau,\mathrm{Dean}}$, mm/s	4.15	8.79
s^+	15	31
h^+	9.1	19
L^+	2500	5300

are in good agreement with the DNS data of Kuroda et al.[11] and Kim[21] at almost the same Reynolds numbers. When $s^+ = 15$, the spanwise difference in the mean velocities is confined to $(y^+ - y_p^+) < 9$. Thus, the riblet surface has a direct influence on the mean velocity distribution only within the viscous sublayer. When $s^+ = 31$, however, the spanwise inhomogeneity extends to $(y^+ - y_p^+) = 25$, so that even the mean velocity distribution in the buffer layer is also affected. The logarithmic profile for $s^+ = 31$ is shifted somewhat downward from that on the smooth wall, and this is the same tendency as in the DNS data of Choi et al.[9] for $s^+ = 40$.

Figure 4 shows the mean velocity distributions at several spanwise locations near the riblet surface. When $s^+ = 15$, U/U_0 is uniformly distributed in the spanwise direction above $y/h = 2$. In the vicinity of the riblet, however, the velocity gradient above the peak is very large, whereas it almost vanishes above the valley. For $s^+ = 31$, U/U_0 is much larger in the valley, but the spanwise variation is also confined to $y/h < 2$. Contours of the streamwise mean velocity in the y-z plane shown in Fig. 5 also demonstrate that the spanwise

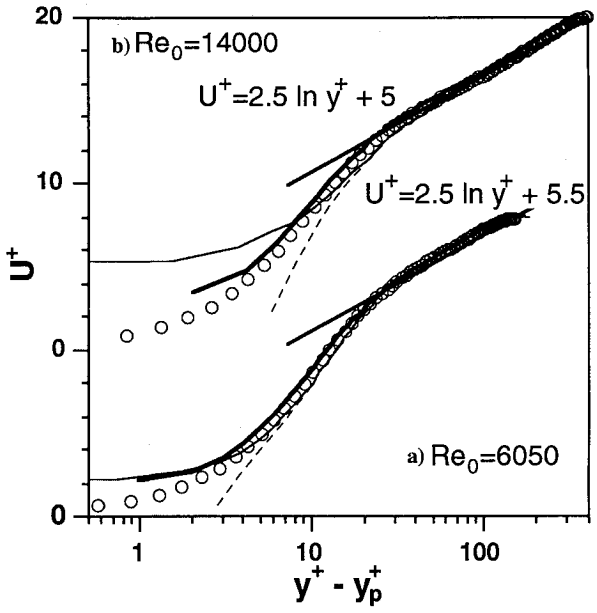

Fig. 3 Mean velocity profiles: ▬, smooth wall; ---, $z/s = 0.0$; ——, $z/s = 0.5$: a) $s^+ = 15$, ○, DNS data of Kuroda et al.[11] at $Re_0 = 5.36 \times 10^3$ and b) $s^+ = 31$, ○, DNS data of Kim[21] at $Re_0 = 1.578 \times 10^4$.

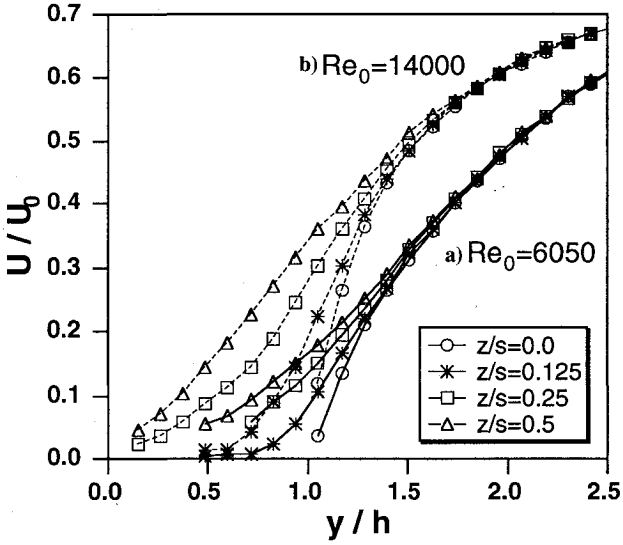

Fig. 4 Streamwise mean velocity distributions near the ribs: a) $s^+ = 15$ and b) $s^+ = 31$.

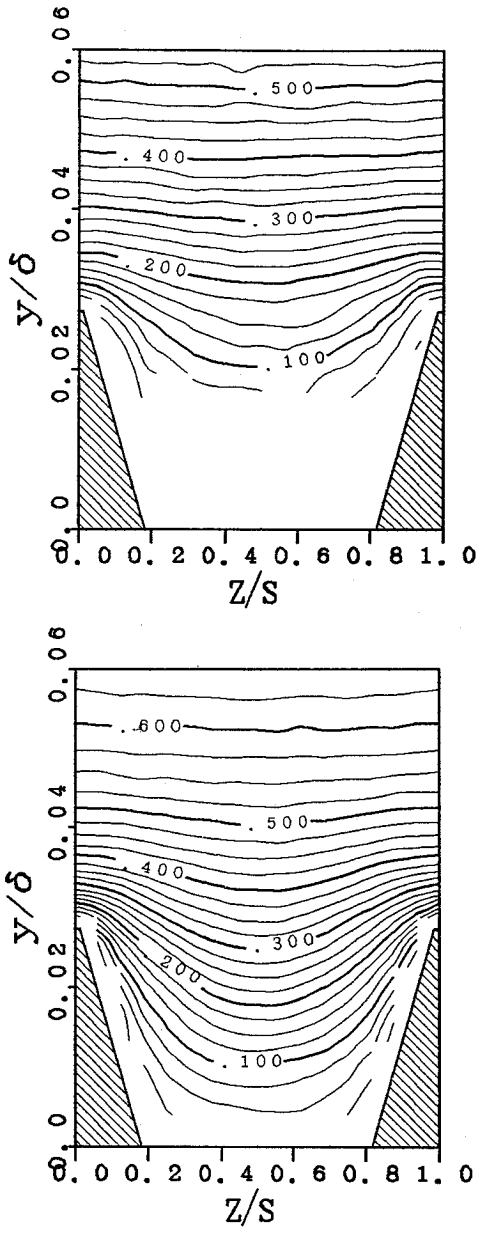

Fig. 5 Contours of streamwise mean velocity U/U_0 near the ribs: a) $s^+ = 15$ and b) $s^+ = 31$.

distributions are uniform at $y/h > 2$. These findings are generally in good agreement with the hot-wire[4,5] and DNS data.[9]

Figure 6 shows the mean velocity vectors in the cross-stream plane. In both cases, the secondary vortical motions upwelling above the peak and downwashing toward the valley are evident. For $s^+ = 15$, their magnitude is rather small and less than 0.1% of the maximum streamwise velocity. On the other hand, for $s^+ = 31$, the secondary flow becomes much more vigorous and as large as 0.8% of U_0. Moreover, the cores of this secondary flow move closer to the ribs. Hence, they should enhance the momentum transport near the ribs and increase the drag in this case. Note that these results should not be interpreted as steady counter-rotating vortices but as an ensemble average of many instantaneous turbulent streamwise vortices that appear randomly but nonuniformly in space near the riblet. Choi et al.[9] recently showed the similar secondary motions in their DNS above a V-shaped riblet. Although the strength of the secondary flow is in close agreement with the present results, its center remains at almost the same position for the two different s^+ values in their simulation. It is also worth noting that Khan[22] predicted similar secondary flows

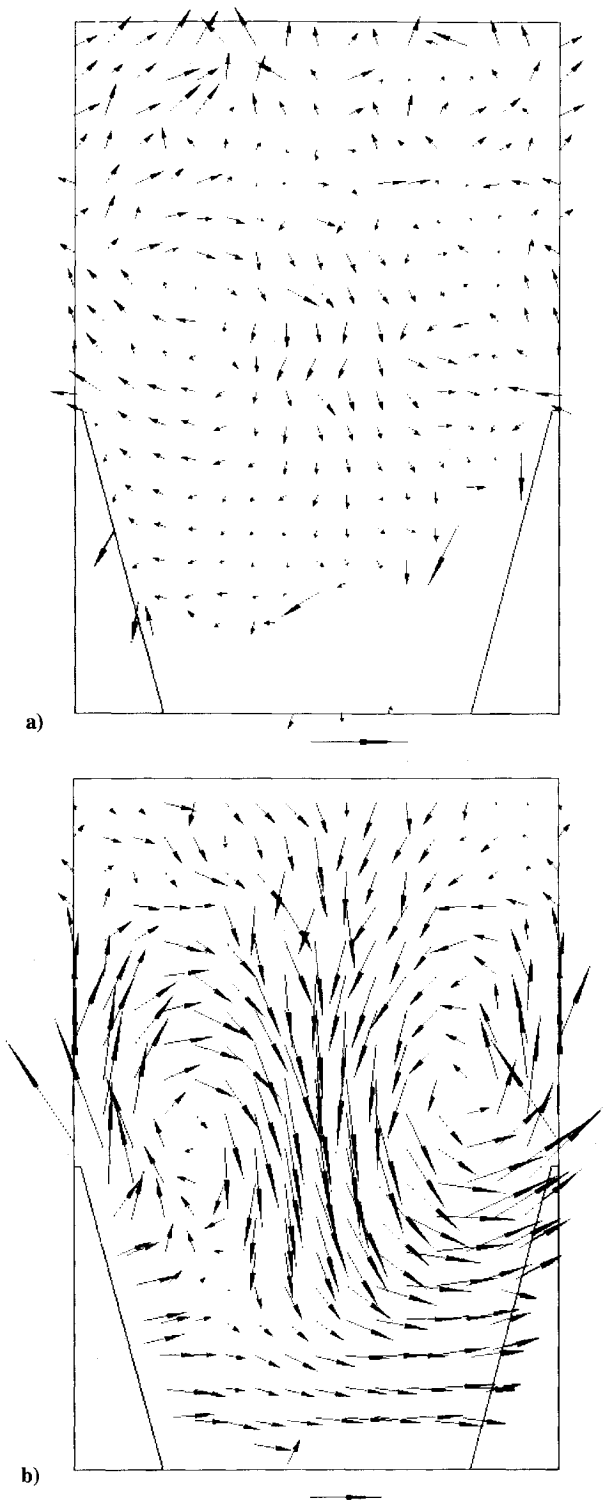

Fig. 6 Mean velocity vectors in the y-z plane: a) $s^+ = 15$ and b) $s^+ = 31$. Each reference vector at the bottom of the figure corresponds to $0.005U_0$.

near the riblet in his mixing-length model calculation, whereas Launder and Li[23] obtained oppositely rotating motions with their second-order closure model.

The distributions of rms velocity fluctuations across the channel are shown in Fig. 7. When $s^+ = 15$, the peak values of all three components are decreased compared with those on the smooth wall. When $s^+ = 31$, u_{rms} is significantly decreased, whereas v_{rms} and w_{rms} are increased in their peak values. In both cases, the spanwise variations are confined in the region close to the ribs, although the difference at the two spanwise locations is greater for $s^+ = 31$. However, Choi et al.[9] reported that, when $s^+ = 40$, the peak u_{rms} value above the riblet tip is increased compared with that on the smooth wall, whereas that above the valley is decreased. It is conjectured that these somewhat different observations should be due to the differences in the s^+ value and the riblet shape. Chu and Karniadakis[12] reported that u_{rms} and w_{rms} exhibit slight bumps deep in the valley, but they are not seen in the present results and the data of Choi et al.[9]

The virtual origin in the wall-normal direction is often used[9,20] when the turbulent statistics on the riblet surface are compared with those on the smooth wall. However, some ambiguity and uncertainty in determining the virtual origin cannot be avoided, especially when experimental data are analyzed. Thus, in the present study, the local streamwise mean velocity is used as the abscissa instead of the distance

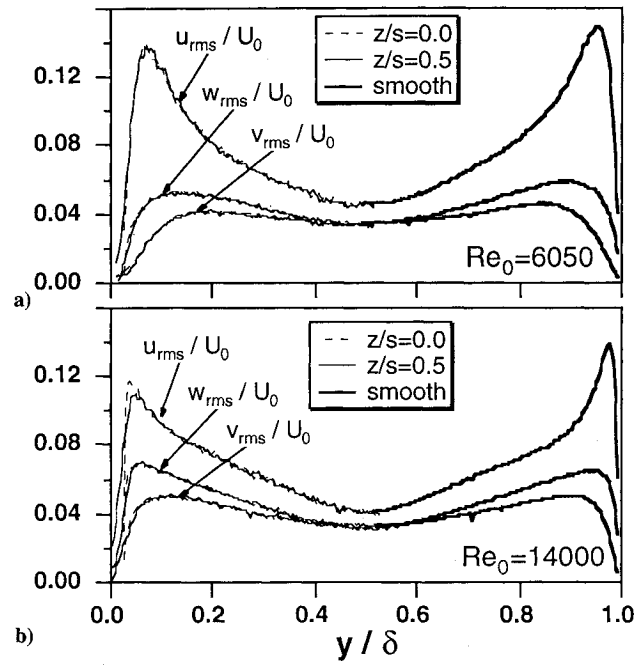

Fig. 7 Turbulent intensity distributions across the channel: a) $s^+ = 15$ and b) $s^+ = 31$.

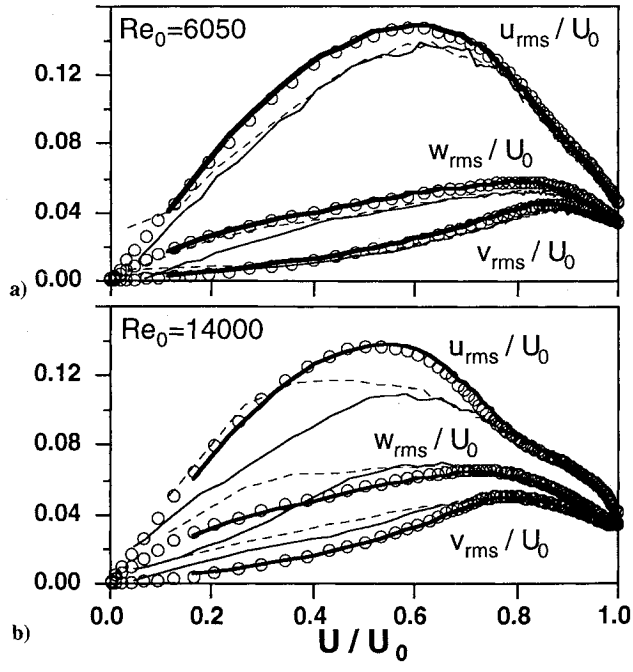

Fig. 8 Turbulent intensity distributions vs U/U_0: a) $s^+ = 15$ and b) $s^+ = 31$. Keys as in Fig. 3.

from the wall. Figure 8 shows the distributions of turbulent intensities vs the local mean velocity. Agreement between the present data near the smooth wall and the DNS data[11,21] is excellent. When $s^+ = 15$, the spanwise variation of the turbulence intensities is confined in the region of $U/U_0 < 0.5$, which corresponds to $y/h < 2$. It is clearly seen that all three components at $U/U_0 < 0.8$ are decreased by about 10% in their peak values. Near the riblet valley, w_{rms} is furthermore decreased. The suppression of the w component was considered to be a major effect of the riblet surface[3,20]; the present result quantitatively confirms the previous deductions. When $s^+ = 31$, u_{rms} is decreased by 30% at the peak value above the valley, but v_{rms} and w_{rms} are increased considerably. Therefore, whether the flow is under the drag reduction or neutral/drag increase condition should be crucial for the alteration of the turbulent statistics above the riblet surface.

Figure 9 shows the diagonal components of the stress anisotropy tensor $[b_{ij} = \overline{u_i u_j}/(2k) - \delta_{ij}/3,\ k = \overline{u_i u_i}/2]$. The present data on the smooth wall are again in excellent agreement with the DNS data.[11,21] For $s^+ = 15$, the diagonal components

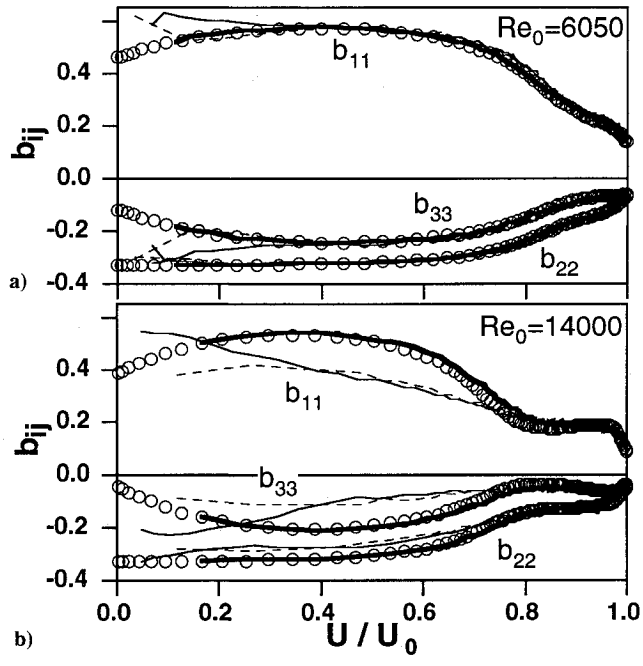

Fig. 9 Diagonal components of the stress anisotropy tensor vs U/U_0: a) $s^+ = 15$ and b) $s^+ = 31$. Keys as in Fig. 3.

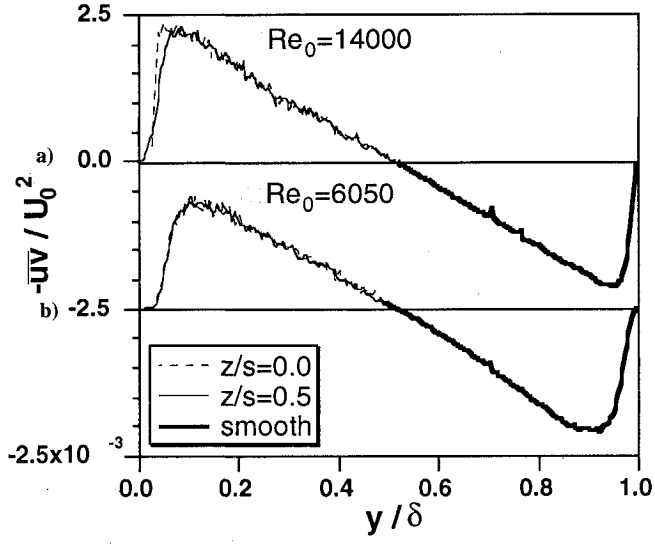

Fig. 10 Distributions of the Reynolds shear stress $-\overline{uv}$ across the channel: a) $s^+ = 15$ and b) $s^+ = 31$. Keys as in Fig. 3.

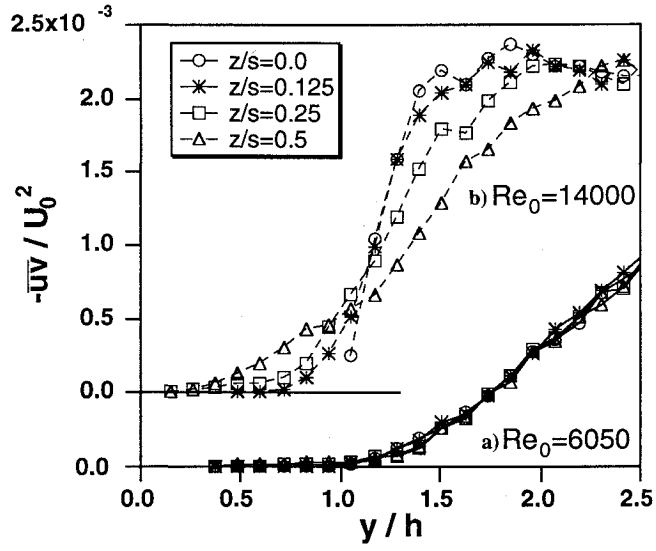

Fig. 11 Distribution of the Reynolds shear stress $-\overline{uv}$ near the ribs: a) $s^+ = 15$ and b) $s^+ = 31$.

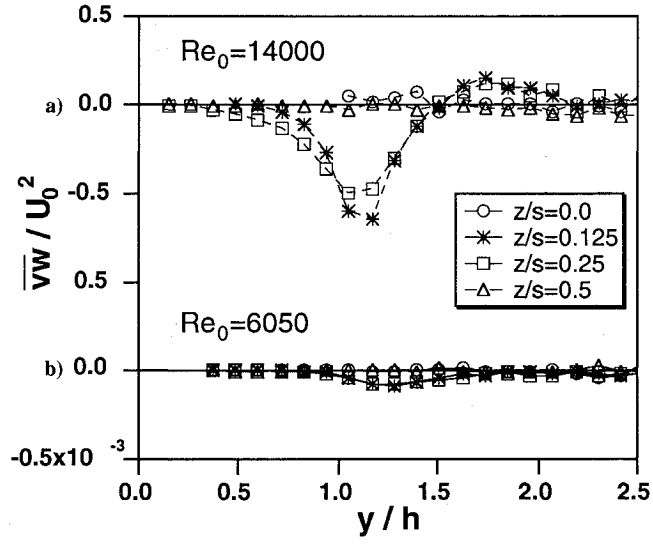

Fig. 12 Distribution of the Reynolds shear stress $\overline{vw}$ near the ribs: a) $s^+ = 15$ and b) $s^+ = 31$.

near the riblet surface are very close to those above the smooth wall. However, in the close vicinity to the valley, b_{11} increases and b_{33} decreases, whereas b_{22} remains unchanged. This fact implies that the mechanism of the intercomponent transfer of turbulent kinetic energy is modified in this region, as is further discussed later. For $s^+ = 31$, the absolute values of all anisotropy measures are decreased, so that the flowfield becomes more isotropic. In the region close to the valley, however, b_{11} increases and b_{33} decreases as in the case of $s^+ = 15$.

The distributions of the Reynolds shear stress $-\overline{uv}$ are shown in Fig. 10. For $s^+ = 15$, $-\overline{uv}$ is markedly decreased, and the maximum Reynolds stress is only 85% of that on the smooth wall. This implies that the drag reduction was actually achieved on the riblet surface under this flow condition. For $s^+ = 31$, the peak value above the riblet wall is even larger than that above the smooth wall, and no drag reduction can be anticipated. Whereas $-\overline{uv}$ is decreased as much as 15% for $s^+ = 15$, the correlation coefficients between u and v, R_{uv}, are not much changed except very close to the ribs, $y/h < 2$ (Ref. 24). This fact, along with b_{ij} shown in Fig. 9, indicates that the structural aspect of turbulence at $s^+ = 15$ should remain almost unchanged from that on the smooth wall. On the other

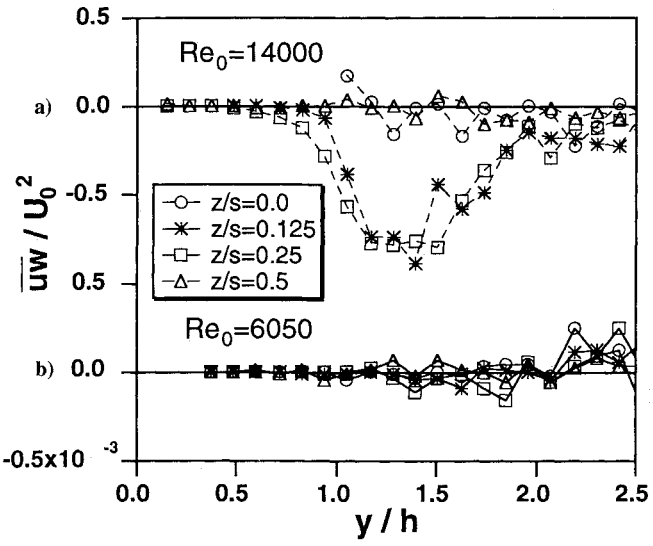

Fig. 13 Distribution of the Reynolds shear stress $\overline{uw}$ near the ribs: a) $s^+ = 15$ and b) $s^+ = 31$.

hand, when $s^+ = 31$, the value of R_{uv} is considerably different from that on the smooth wall throughout the flowfield.[24]

Figure 11 shows the distributions of $-\overline{uv}$ at several spanwise locations near the riblet surface. When $s^+ = 15$, it is apparent that $-\overline{uv}$ is uniform in the spanwise direction even in the vicinity of the ribs. Note that $-\overline{uv}$ is substantially zero inside the valley. When $s^+ = 31$, the spanwise variation of $-\overline{uv}$ is quite large, and the Reynolds stress even inside the valley is not negligible.

The distributions of $\overline{vw}$ near the riblet surface are shown in Fig. 12. In both cases, negative peaks are evident close to the ribs, although the magnitude is much larger for $s^+ = 31$ than for $s^+ = 15$. As one expects from the spanwise symmetry of the flowfield with respect to the plane of $z/s = 0.5$, $\overline{vw}$ at $0.5 < z/s < 1.0$ exhibits a positive peak.[24] The signs of these peaks indicate that fluid motions approaching the riblet tip are attenuated by the presence of the ribs. Figure 13 shows the distributions of $\overline{uw}$. A similar peak is evident for $s^+ = 31$, whereas there is seen no substantial trend for $s^+ = 15$. Benhalilou et al.[25] also reported a significant spanwise variation of $\overline{uw}$ for $s^+ = 30$.

B. Two-Point Correlations

Among various coherent structures near the wall, the so-called low-speed streak is one of the distinct features.[26] The mean spanwise spacing on the smooth wall is known to be about 100 viscous lengths.[26,27] On the riblet surface, Gallagher and Thomas[28] reported that the spanwise correlation length increased by 15–30%, and later Bacher and Smith[29] reported the same observation, but Pulles[6] obtained an opposite result. Note that, in drag-reducing polymer solutions, the spanwise spacing of the streaky structures is markedly increased.[30] Chu and Karniadakis[12] also reported the spanwise two-point correlations. However, there are noticeable discrepancies between their results and the DNS data of channel flow[10,11] even at the channel centerline; their results seem to be erroneous. The spanwise two-point correlations presently calculated are shown in Fig. 14. The elevation from the riblet surface is chosen in such a way that the mean velocity is equal to that at $y^+ = 14$ above the smooth wall. When $s^+ = 15$, every two-point correlation on the riblet surface is in good agreement with that on the smooth wall as well as the channel flow DNS data[11] as shown in Fig. 14a. Therefore, the spanwise dimension of the large eddy structure should not be changed by the riblet under the drag-reducing condition. When $s^+ = 31$, $R_{uu}(\Delta z)$ and $R_{ww}(\Delta z)$ on the riblet surface show almost the same behavior as on the smooth wall, but the first negative peak in $R_{vv}(\Delta z)$ is no longer evident as seen in Fig. 14b.

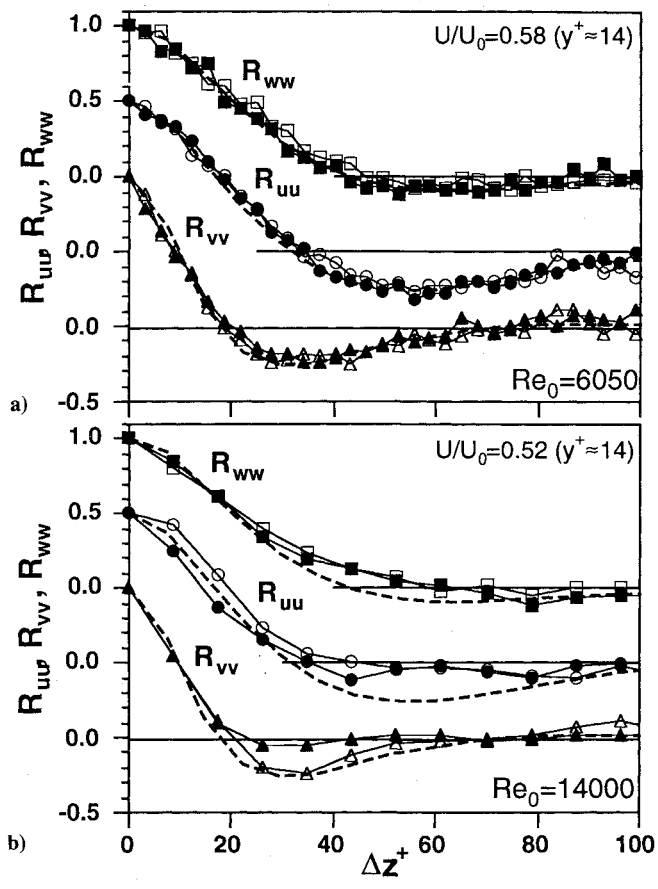

Fig. 14 Two-point correlations in the spanwise direction at $y^+ \approx 14$: a) $s^+ = 15$ and b) $s^+ = 31$. Open symbol, smooth surface; solid symbol, riblet surface; and ---, DNS data of Kuroda et al.[11] at $y^+ = 13.5$.

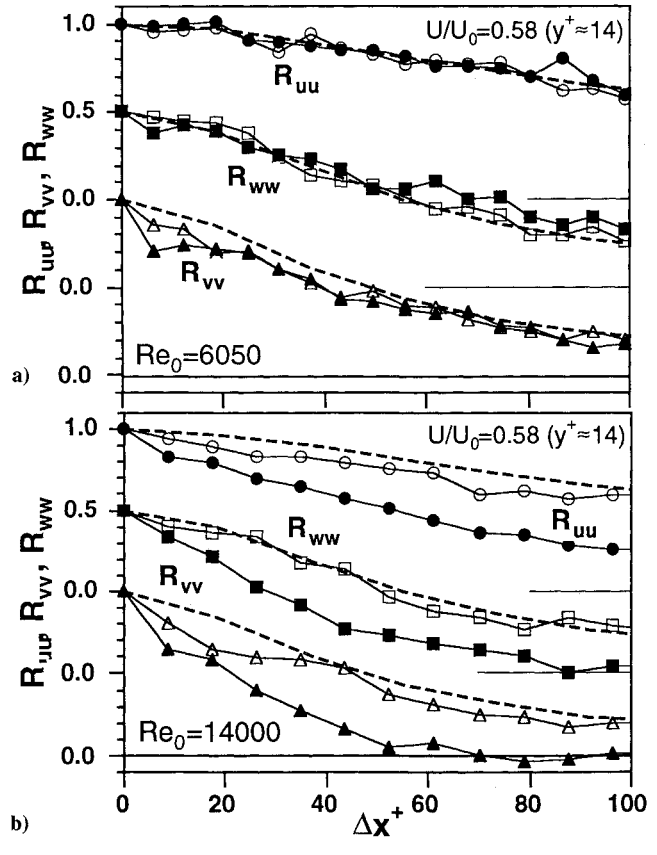

Fig. 15 Two-point correlations in the streamwise direction at $y^+ \approx 14$: a) $s^+ = 15$ and b) $s^+ = 31$. Keys as in Fig. 14.

Figure 15a shows the streamwise two-point correlations for $s^+ = 15$. Again, their distributions are in accordance with those on the smooth wall and the DNS data.[11] On the other hand, for $s^+ = 31$, they rapidly diminish within a smaller streamwise distance as seen in Fig. 15b. This fact implies that, for $s^+ = 31$, the streamwise persistence of the streaky structures becomes shorter on the riblet surface. Although it is not shown here, the peaky value of the shear parameter $S^*[= 2(\partial U/\partial y)(k/\epsilon)]$ is leveled off[24] for $s^+ = 31$. Lee et al.[31] and Kuroda et al.[11] pointed out from their numerical simulation that the near-wall streaky structures are produced when S^* is sufficiently large. Therefore, the aforementioned fact should have a close relationship to the reduction of the streamwise correlation length.

C. Budget of the Reynolds Stresses

In Sec. III.A, it is conjectured that the riblet surface would alter the intercomponent transfer mechanism of the turbulent kinetic energy in the near-wall region. In this section, we estimate each term in the Reynolds stress transport equation on the riblet to further clarify this effect.

For an incompressible flow of constant physical properties, the transport equation of turbulent kinetic energy leads to

$$P_k + T_k + D_k + \Pi_k - \epsilon + A_k = 0 \tag{1}$$

where

P_k = production, $-\overline{u_i u_j}\, U_{i,j}$
T_k = turbulent diffusion, $-\frac{1}{2}(\overline{u_i u_i u_j})_{,j}$
D_k = viscous diffusion, $\nu k_{,ii}$
Π_k = pressure diffusion, $-(\overline{pu_i})_{,i}$
ϵ = dissipation rate, $\nu \overline{u_{i,j} u_{i,j}}$
A_k = advection, $-Dk/Dt$

Each term is nondimensionalized by U_0 and δ. The terms of P_k, T_k, D_k, and A_k can be calculated directly from the database obtained by the present measurement. When Π_k is assumed negligibly small, ϵ can be estimated as a residual:

$$\epsilon = -(P_k + T_k + D_k + A_k) \tag{2}$$

The present results on the smooth wall are confirmed to be in good agreement with the DNS data[11,21] of channel flow, so that they would be competent for this secondary data reduction.[24,32]

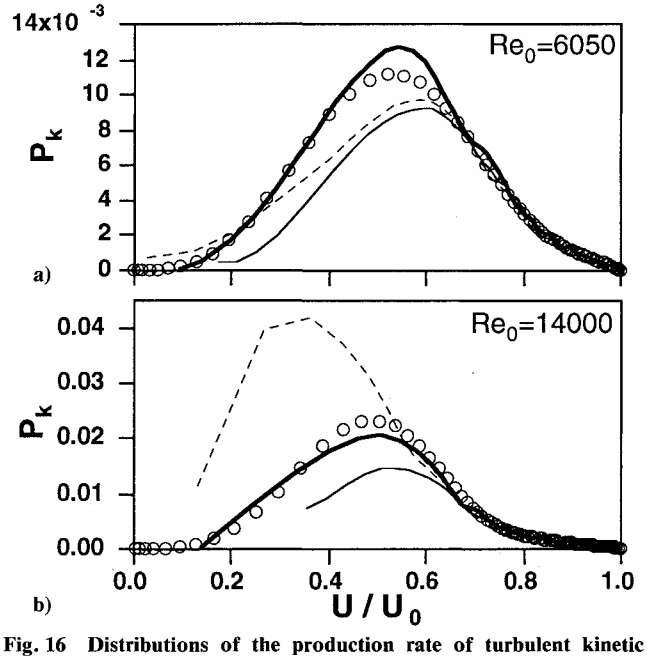

Fig. 16 Distributions of the production rate of turbulent kinetic energy P_k: a) $s^+ = 15$ and b) $s^+ = 31$. Keys as in Fig. 3.

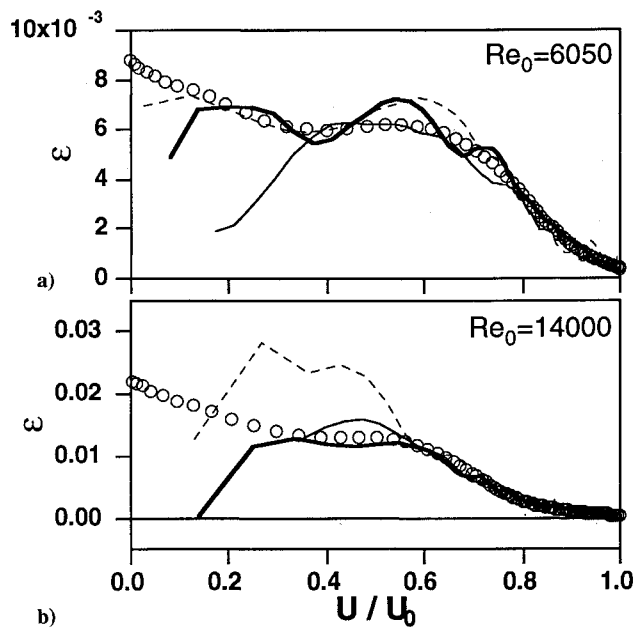

Fig. 17 Distributions of the dissipation rate of turbulent kinetic energy ϵ: a) $s^+ = 15$ and b) $s^+ = 31$. Keys as in Fig. 3.

Figure 16 shows the distributions of P_k. When $s^+ = 15$, P_k is appreciably decreased near the riblet surface. The difference at the two spanwise locations is small in this case. When $s^+ = 31$, the spanwise inhomogeneity is significant; P_k above the riblet peak is very large owing to the steep mean velocity gradient, whereas that above the valley is considerably suppressed. It is noted that $\partial U/\partial y$ is the major term in P_k and the contribution of the spanwise mean velocity gradient, e.g., $\partial U/\partial z$, is negligibly small in both cases. This is in general agreement with Benhalilou et al.[8] and Choi et al.[9]

Figure 17 shows the distribution of ϵ. When $s^+ = 15$, ϵ above the riblet peak is almost equal to that on the smooth wall, whereas ϵ above the valley is markedly decreased. For $s^+ = 31$, ϵ has a large value near the riblet peak. Although it is not shown here, the magnitude of the diffusion terms is decreased on the riblet wall of $s^+ = 15$ (Ref. 32). Note that the advection term A_k is much smaller than P_k or ϵ in both cases.[32]

The Reynolds stress transport equation is derived as follows:

$$P_{ij} + T_{ij} + D_{ij} + \phi_{ij} - \epsilon_{ij} + A_{ij} = 0 \tag{3}$$

where

P_{ij} = production, $-\overline{u_i u_k}\, U_{j,k} - \overline{u_j u_k}\, U_{i,k}$
T_{ij} = turbulent diffusion, $-(\overline{u_i u_j u_k})_{,k}$
D_{ij} = viscous diffusion, $\nu(\overline{u_i u_j})_{,kk}$
ϕ_{ij} = velocity pressure-gradient correlation, $-(\overline{u_i p_{,j}} + \overline{u_j p_{,i}})$
ϵ_{ij} = dissipation rate, $2\nu \overline{u_{i,k} u_{j,k}}$
A_{ij} = advection, $-D\overline{u_i u_j}/Dt$

Again, we can calculate P_{ij}, T_{ij}, D_{ij}, and A_{ij} directly from our database, so that we have two unknown terms, ϕ_{ij} and ϵ_{ij}. In the present study, ϵ_{ij} is estimated from ϵ using the following formula proposed by Hallbäck et al.[33]:

$$\epsilon_{ij} = \epsilon(e_{ij} + \tfrac{1}{3}\delta_{ij}) \tag{4}$$

where

$$e_{ij} = [1 - 2\alpha(2II + \tfrac{1}{3})]b_{ij} - 2\alpha(b_{ik}b_{kj} + \tfrac{2}{3}\delta_{ij}II)$$

$$II = -\tfrac{1}{2}b_{ij}b_{ji}$$

The constant α was originally determined to be 0.75 by the rapid distortion theory, but we use $\alpha = 0.25$, which was found

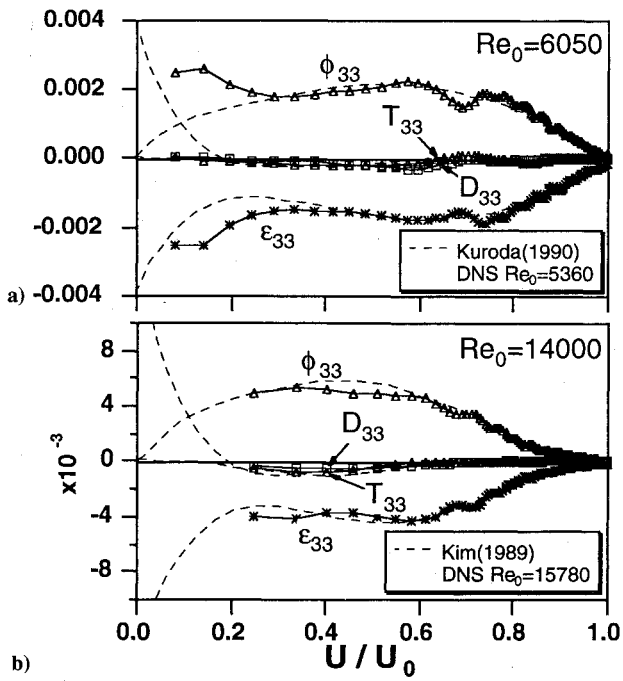

Fig. 18 Terms in the budget equation of $\overline{w}^2$ on the smooth wall: a) $Re_0 = 6.05 \times 10^3$ and b) $Re_0 = 1.4 \times 10^4$.

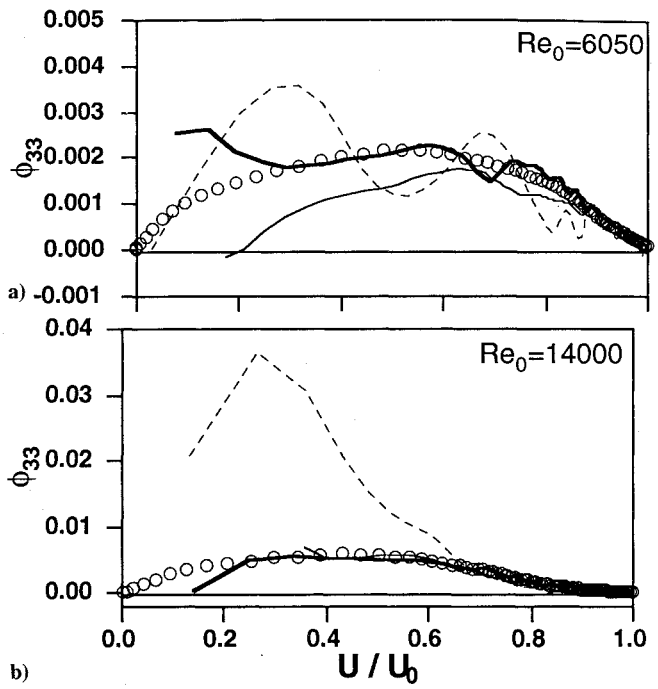

Fig. 19 Distribution of the velocity pressure-gradient correlation term in the $\overline{w^2}$ transport equation vs U/U_0: a) $s^+ = 15$ and b) $s^+ = 31$. Keys as in Fig. 3.

to be the optimum for fitting the DNS data of channel flows.[11,21] With Eqs. (3) and (4), ϕ_{ij} is estimated as a residual.

The terms in the budget of $\overline{w^2}$ on the smooth surface are shown in Fig. 18. The present results are again in good agreement with the DNS data,[11,21] so that the present method of data reduction can be validated. It is obvious that ϕ_{33} is almost balanced against ϵ_{33}, and the diffusion terms are negligibly small except very close to the wall.

Figure 19 shows the distributions of ϕ_{33} on the riblet walls. It is apparent in both cases that ϕ_{33} is markedly decreased near the riblet valley. This fact quantitatively confirms that the kinetic energy transfer from the streamwise to spanwise components is substantially impeded in the vicinity of the valley. Since the redistribution process of the turbulent kinetic energy is crucial for the sustenance of turbulence, this fact should be an important dynamical aspect in understanding the drag reduction mechanism above the riblet surface.

IV. Drag Reduction Mechanism

In this section, we focus on several possible drag reduction mechanisms proposed based on the measured turbulent statistics.

Vukoslavčević et al.[4] anticipated that the skin-friction reduction in the riblet valleys might be sufficient to overcome the skin-friction increase near riblet tips. Djenidi et al.[34] reported a 2–3% drag reduction even in a laminar boundary layer. However, Choi et al.[35] claimed that the grid resolution is not sufficient in the calculation of Djenidi et al.,[34] and they showed from their finite difference computations that the drag should be increased in the laminar riblet channel flow. Suzuki[32] also confirmed this conclusion through finite element computations. Therefore, it is not likely that the decrease in the local wall shear stress in the valley, which is caused purely by the viscous retardation, would collectively benefit more than the increase in the wetted area on the riblet surface.

Bacher and Smith[29] conjectured that the interaction between the turbulent streamwise vortices and the secondary vortices induced inside the valley should be a key mechanism for the drag reduction. However, it is evident from Figs. 11–13 that all three Reynolds shear stress components are almost zero inside the valley for $s^+ = 15$. This fact suggests that the flowfield inside the valley is dominated by the viscous force and dynamically inactive under the drag-reducing condition. Thus, the aforementioned mechanism proposed by Bacher and Smith[29] does not seem plausible.

On the other hand, the vigorous turbulent motion in the valley does exist under the drag-increasing condition; all the Reynolds stresses are not negligible inside the valley as shown in Figs. 11–13. Tullis and Pollard[36] found in their "time-dependent" simulations that rapidly decaying secondary motions exist in the valley for $s^+ = 33.3$, whereas those motions are extremely weak for $s^+ = 16.7$. Clark[37] also reported cellular crossflows in the valley of $s^+ = 30$ in his flow visualization. These findings are qualitatively in good agreement with the present results.

Choi et al.[9] examined instantaneous turbulent structures in their DNS flowfield. They found that, when $s^+ = 20$, the streamwise vortical structures of about 30 viscous wall units in diameter stay above the riblets, whereas they were sometimes submerged into the valley when $s^+ = 40$. They attributed the drag increase at $s^+ = 40$ to the presence of vortices in the valley, since these vortices should bring about high wall shear regions inside the valley. Their findings also support the present observations mentioned earlier.

Choi[3] and Bechert and Bartenwerfer[20] separately suggested that the suppression of the w component might be a major effect of the riblet surface. The present results show that the spanwise fluctuation near the riblet surface is markedly decreased by the suppression of the turbulent kinetic energy transfer from the u to w components near the valley, and this result quantitatively confirms their suggestions.

Recently, Kasagi and Ohtsubo[38] and Kasagi et al.[39] employed three-dimensional computer-aided visualization to investigate near-wall quasicoherent structures in a DNS database of channel flow[11] and examined instantaneous spatial distributions of the terms in the transport equations of Reynolds stresses. They found that these balance terms were distributed intermittently in space but closely associated with the quasistreamwise vortical structures near the wall. Thus, they reached the same conclusion as Robinson et al.[40] that these vortical structures should play a primary role in the near-wall turbulent mechanism. Moreover, Kasagi and Ohtsubo[38] and Kasagi et al.[39] reported that the redistribution mechanism adjacent to the wall is deeply related to the sweep motion,

which occurs on the downwash side of the streamwise vortex; a local high-pressure region is produced on the wall, and the turbulent kinetic energy is converted from u and v to w. The present results indicate this splatting[41] mechanism should be somehow attenuated on the riblet surface. This should cause the reduction in the streamwise vorticity fluctuation, since the wall-normal derivative of the w component is a major contributor to the streamwise vorticity. Choi et al.[9] reported that the vorticity fluctuations were decreased on the riblet surface of $s^+ = 20$, and this is in favor of the preceding argument. It is further conjectured that the decrease in the streamwise vorticity fluctuations should be brought about through some suppression effect on the vortex regeneration mechanism[42,43] and/or vortex damping due to the pressure reflection from the riblet surface.

V. Conclusions

The turbulent flowfield above the riblet surface was measured by using the three-dimensional particle tracking velocimetry. The turbulent statistics of all three velocity components were obtained. The two-point correlations and budgets of the turbulent kinetic energy and Reynolds stresses were also examined. The following conclusions are derived:

1) The spanwise variation of the streamwise mean velocity is confined in the region very close to the riblet surface, say $y/h < 2$, regardless of the riblet spacing s^+. However, the turbulent statistics and the flow structures strongly depend on s^+.

2) When $s^+ = 15$, although the turbulent intensities and the Reynolds shear stress are decreased near the riblet surface, the structural aspect of turbulence remains almost unchanged except in the region very close to the ribs. The distributions of two-point correlations also show that the near-wall coherent structures have almost the same dimensions as those on the smooth wall. In the vicinity of the valley, however, the turbulent energy redistribution from the streamwise to spanwise components is impeded. This suggests the reduction in the streamwise vorticity, and hence the drag reduction mechanism is considered closely related with the suppression of near-wall vortex generation and/or damping of the vortices.

3) When $s^+ = 31$, the flowfield becomes more isotropic. The vigorous cross-stream secondary motions found close to the ribs should enhance the momentum transport and increase the skin friction. It is also found from the correlation length that the streamwise persistence of the streaky structures should become considerably shorter in this case.

Acknowledgments

The financial supports through the Grants-in-Aid for General Scientific Research (No. 04452140) and for Encouragement of Young Scientists (No. 02952138) by the Ministry of Education, Science and Culture are acknowledged. Also, the authors are grateful to R. Funatsu (Instrument Division, Hitachi Ltd.) for his valuable suggestions and cooperation in designing and manufacturing the riblet surface.

References

[1]Walsh, M. J., "Turbulent Boundary Layer Drag Reduction Using Riblets," AIAA Paper 82-0169, Jan. 1982.

[2]Walsh, M. J., "Riblets," *Viscous Drag Reduction in Boundary Layers,* edited by D. M. Bushnell and J. N. Hefner, Vol. 123, Progress in Astronautics and Aeronautics, AIAA, Washington, DC, 1990, pp. 203–261.

[3]Choi, K.-S., "Near-Wall Structure of a Turbulent Boundary Layer with Riblets," *Journal of Fluid Mechanics,* Vol. 208, 1989, pp. 417–458.

[4]Vukoslavčević, P., Wallace, J. M., and Balint, J.-L., "Viscous Drag Reduction Using Streamwise-Aligned Riblets," *AIAA Journal,* Vol. 30, No. 4, 1991, pp. 1119–1122.

[5]Park, S.-R., and Wallace, J. M., "Flow Alteration and Drag Reduction by Riblets in a Turbulent Boundary Layer," *AIAA Journal,* Vol. 32, No. 1, 1994, pp. 31–38.

[6]Pulles, C. J. A., "Drag Reduction of Turbulent Boundary Layers by Means of Grooved Surfaces," Ph.D. Dissertation, Eindhoven Univ. of Technology, The Netherlands, 1988.

[7]Nakao, S., "Turbulent Boundary Layer Developing on Drag Reduction Riblet," *Theoretical and Applied Mechanics,* Vol. 39, 1990, pp. 303–308.

[8]Benhalilou, M., Anselmet, F., and Fulachier, L., "Experimental Investigation of a Turbulent Boundary Layer Manipulated by a Ribbed Surface," *Proceedings of the 9th Symposium on Turbulent Shear Flows,* Kyoto Univ., Japan, Aug. 1993, pp. P107.1–P107.4.

[9]Choi, H., Moin, P., and Kim, J., "Direct Numerical Simulation of Turbulent Flow over Riblets," *Journal of Fluid Mechanics,* Vol. 255, 1993, pp. 503–539; also Stanford Univ., CTR Manuscript 137, Stanford, CA, July 1992.

[10]Kim, J., Moin, P., and Moser, R., "Turbulent Statistics in Fully Developed Channel Flow at Low Reynolds Number," *Journal of Fluid Mechanics,* Vol. 177, 1987, pp. 133–166.

[11]Kuroda, A., Kasagi, N., and Hirata, M., "Direct Numerical Simulation of Turbulent Plane Couette-Poiseuille Turbulent Flows: Effect of Mean Shear on the Near Wall Turbulence Structures," *Proceedings of the 9th Symposium on Turbulent Shear Flows,* Kyoto Univ., Japan, Aug. 1993, pp. 8.4.1–8.4.6.

[12]Chu, D. C., and Karniadakis, G. E., "A Direct Numerical Simulation of Laminar and Turbulent Flow over Riblet-Mounted Surfaces," *Journal of Fluid Mechanics,* Vol. 250, 1993, pp. 1–42.

[13]Kasagi, N., and Nishino, K., "Probing Turbulence with Three-Dimensional Particle-Tracking Velocimetry," *Experimental Thermal and Fluid Science,* Vol. 4, No. 5, 1991, pp. 601–612.

[14]Kasagi, N., and Sata, Y., "Recent Developments in Three-Dimensional Particle Tracking Velocimetry," *Proceedings of the 6th International Symposium on Flow Visualization* (Yokohama, Japan), Springer-Verlag, Berlin, 1992, pp. 832–837.

[15]Nishino, K., and Kasagi, N., "Turbulence Statistics Measurement in a Two-Dimensional Channel Flow Using a Three-Dimensional Particle Tracking Velocimeter," *Proceedings of the 7th Symposium on Turbulent Shear Flows,* Stanford Univ., Stanford, CA, Aug. 1989, pp. 22.1.1–22.1.6.

[16]Sata, Y., and Kasagi, N., "Improvement Toward High Measurement Resolution in Three-Dimensional Particle Tracking Velocimetry," *Proceedings of the 6th International Symposium on Flow Visualization* (Yokohama, Japan), Springer-Verlag, Berlin, 1992, pp. 792–796.

[17]Dean, R. B., "Reynolds Number Dependence of Skin Friction and Other Bulk Flow Variables in Two-Dimensional Rectangular Duct Flow," *Transactions of the ASME, Journal of Fluids Engineering,* Vol. 100, June 1978, pp. 215–223.

[18]McEligot, D. M., "Measurement of Wall Shear Stress in Accelerating Turbulent Flows," Max-Planck-Institüt für Strömungsforschung, Bericht 109, Göttingen, Germany, 1984.

[19]Nishino, K., Kasagi, N., and Hirata, M., "Three-Dimensional Particle Tracking Velocimetry Based on Automated Digital Image Processing," *Transactions of the ASME, Journal of Fluids Engineering,* Vol. 111, Dec. 1989, pp. 384–391.

[20]Bechert, D. W., and Bartenwerfer, M., "The Viscous Flow on Surfaces with Longitudinal Ribs," *Journal of Fluid Mechanics,* Vol. 206, 1989, pp. 105–129.

[21]Kim, J., unpublished work, 1989.

[22]Khan, M. M. S., "A Numerical Investigation of the Drag Reduction by Riblet-Surfaces," AIAA Paper 86-1127, May 1986.

[23]Launder, B. E., and Li, S. P., "On the Prediction of Flow over Riblets via 2nd-Moment Closure," *Near-Wall Turbulent Flows,* edited by R. M. C. So, C. G. Speziale, and B. E. Launder, Elsevier, Amsterdam, 1993, pp. 739–748.

[24]Suzuki, Y., and Kasagi, N., "On the Turbulent Drag Reduction Mechanism above a Riblet Surface," AIAA Paper 93-3257, July 1993.

[25]Benhalilou, M., Anselmet, F., Liandrat, J., and Fulachier, L., "Experimental and Numerical Investigation of a Turbulent Boundary Layer over Riblets," *Proceedings of the 8th Symposium on Turbulent Shear Flows,* Tech. Univ. of Munich, Germany, Aug. 1991, pp. 18.5.1–18.5.6.

[26]Kline, S. J., Reynolds, W. C., Schraub, F. A., and Runstadler, P. W., "The Structure of Turbulent Boundary Layers," *Journal of Fluid Mechanics,* Vol. 30, 1967, pp. 741–773.

[27]Smith, C. R., and Metzler, S. P., "The Characteristics of Low-Speed Streaks in the Near-Wall Region of a Turbulent Boundary Layer," *Journal of Fluid Mechanics,* Vol. 129, 1983, pp. 27–54.

[28]Gallagher, J. A., and Thomas, A. S. W., "Turbulent Boundary Layer Characteristics over Streamwise Grooves," AIAA Paper 84-2185, Aug. 1984.

[29]Bacher, E. V., and Smith, C. R., "Turbulent Boundary-Layer Modification by Surface Riblets," *AIAA Journal,* Vol. 24, No. 8, 1986, pp. 1382–1385.

[30]Virk, P. S., "Drag Reduction Fundamentals," *AIChE Journal,* Vol. 21, No. 4, 1975, pp. 625–656.

[31]Lee, M. J., Kim, J., and Moin, P., "Structure of Turbulence at

High Shear Rate," *Journal of Fluid Mechanics,* Vol. 216, 1990, pp. 561–583.

[32]Suzuki, Y., "Drag Reduction Mechanism Above a Riblet Surface," Dr. Eng. Thesis, Dept. of Mechanical Engineering, Univ. of Tokyo, Tokyo, Japan, 1993 (in Japanese).

[33]Hallbäck, M., Groth, J., and Johansson, A. V., "An Algebraic Model for Nonisotropic Turbulent Dissipation Rate in Reynolds Stress Closures," *Physics of Fluids A,* Vol. 2, No. 10, 1990, pp. 1859–1866.

[34]Djenidi, L., Liandrat, J., Anselmet, F., and Fulachier, L., "Viscous Effects in Drag Reduction over Riblets," *Drag Reduction in Fluid Flows: Techniques for Friction Control,* edited by R. H. J. Sellin and R. T. Moses, Ellis Horwood, Chichester, England, UK, 1989, pp. 35–41.

[35]Choi, H., Moin, P., and Kim, J., "On the Effects of Riblets in Fully Developed Laminar Channel Flow," *Physics of Fluids A,* Vol. 3, No. 8, 1991, pp. 1892–1896.

[36]Tullis, S., and Pollard, A., "A Numerical Investigation of the Turbulent Flow over V and U Groove Riblets Using a Viscous Wall Region Model," *Near-Wall Turbulent Flows,* edited by R. M. C. So, C. G. Speziale, and B. E. Launder, Elsevier, Amsterdam, 1993, pp. 761–770.

[37]Clark, D. G., "Boundary Layer Flow Visualization Patterns on a Riblet Surface," *Turbulence Control by Passive Means,* edited by E. Coustols, Kluwer, Dordrecht, The Netherlands, 1990, pp. 79–96.

[38]Kasagi, N., and Ohtsubo, Y., "Direct Numerical Simulation of Low Prandtl Number Thermal Field in a Turbulent Channel Flow," *Turbulent Shear Flows 8,* Springer-Verlag, Berlin, 1993, pp. 97–119.

[39]Kasagi, N., Sumitani, Y., Suzuki, Y., and Iida, O., "On the Kinematics of the Quasi-Coherent Vortical Structure in Near-Wall Turbulence," *Proceedings of the 3rd World Conference on Experimental Heat Transfer, Fluid Mechanics and Thermodynamics,* edited by M. D. Kelleher, R. K. Shah, K. R. Sreenivasan, and Y. Joshi, Elsevier, Amsterdam, 1993, pp. 235–242; also *International Journal of Heat and Fluid Flow* (submitted for publication).

[40]Robinson, S. K., Kline, S. J., and Spalart, P. R., "Quasi-Coherent Structures in the Turbulent Boundary Layer: Part II. Verification and New Information from a Numerically Simulated Flat-Plate Layer," *Near Wall Turbulence,* edited by S. J. Kline and N. H. Afgan, Hemisphere, Washington, DC, 1990, pp. 218–247.

[41]Moin, P., and Kim, J., "Numerical Investigation of Turbulent Channel Flow," *Journal of Fluid Mechanics,* Vol. 118, 1982, pp. 341–377.

[42]Brooke, J. W., and Hanratty, T. J., "Origin of Turbulence-Producing Eddies in a Channel Flow," *Physics of Fluids A,* Vol. 5, No. 4, 1993, pp. 1011–1022.

[43]Hamilton, J. M., Kim, J., and Waleffe, F., "Regeneration of Near-Wall Turbulence Structures," *Proceedings of the 9th Symposium on Turbulent Shear Flows,* Kyoto Univ., Japan, Aug. 1993, pp. 11.5.1–11.5.6.